

# Simulation of Electric Vehicles Combining Structural and Functional Approaches

L. I. Silva<sup>†\*</sup>, G. A. Magallán\*, P. M. De la Barrera\*, C. H. De Angelo\* and G. O. García\*

**Abstract** – In this paper the construction of a model that represents the behavior of an Electric Vehicle is described. Both the mechanical and the electric traction systems are represented using Multi-Bond Graph structural approach suited to model large scale physical systems. Then the model of the controllers, represented with a functional approach, is included giving rise to an integrated model which exploits the advantages of both approaches. Simulation and experimental results are aimed to illustrate the electromechanical interaction and to validate the proposal.

**Keywords:** Modeling and simulation, Electric vehicles, Multi-bond graph

## 1. Introduction

Transportation solutions have been thoroughly investigated to improve fuel economy and reduce vehicle emissions. Electric Vehicles (EV) have been proposed as possible solutions to meet these goals, see Fig. 1.

Modeling and Simulation are key tasks for testing novel concepts. They help in the design stage allowing the evaluation of different vehicle configurations, inexpensively and without implementing a prototype. A well detailed revision of vehicle models and their features is given in [1]. An overview of EVs with a focus on hybrid configurations and energy management is discussed in [2].

Vehicle models are classified as steady-state, dynamic and quasi-steady-state. In steady-state models transients are neglected and require less computation power than dynamic models which are physic-based and reproduce transient evolutions. An intermediate solution is a quasi-steady-state model. Another classification is based on the calculation direction: Forward models follow the engine-to-wheel direction whereas backward models follow the wheel-to-engine relations. Generally, dynamic models are used in forward calculation and hardware-in-the-loop simulation [3].

Once the model of the vehicle is defined according to the application, the representation of the model can be accomplished with a functional or structural approach [4]. In a functional approach the connections between sub-systems are virtual links. It gives an overall description of the system and is used in applications oriented to its control. On the other hand, structural approaches are based on the topology of the real system and the links respond to

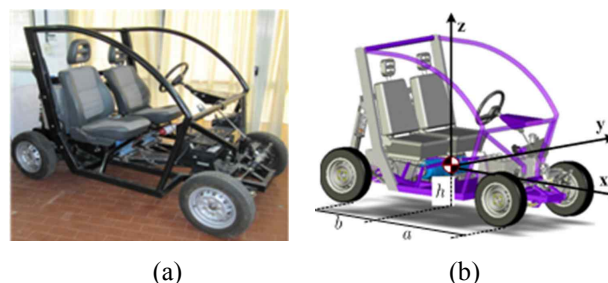


**Fig. 1.** (a) Vehicle prototype; (b) Vehicle geometry in CAD design.

a physical connection. Hence a direct correspondence between the system under analysis and its representation is generated. Structural approaches are useful for system design and its analysis in faulty conditions.

In applications such as those addressed in this paper, it is convenient to resort to energy-based approaches. They explicitly define the energy flow and/or power interaction between components. Some energy-based approaches are:

**Bond graphs** (BG) allows interconnecting sub-systems based on their power flow [5] and facilitates the interconnection of multi domain systems [6]. BG contains dissipative, accumulative, conversion elements and junctions. Elements are interconnected by bonds that carry the exchange variables (general flow and effort) and allow an easy visualization of the physical system topology and power flow.

**Multi Bond graphs** (MBG) [7] is a vectorial extension of standard BG. It is also a non-causal approach suited to model large scale multi domain physical systems.

**Power Flow Diagrams** (PFD) [8] is based on splitting the bond to differentiate flow and effort variables to better interpret the system. New pictograms are defined to highlight the different elements in the system. PFDs have been used to study electric drives and traction systems [9].

**Energetic Macroscopic Representation** (EMR) [10] makes apparent the power interchange between subsystems.

<sup>†</sup> Corresponding Author: Grupo de Electrónica Aplicada, Facultad de Ingeniería, Universidad Nacional de Río Cuarto, Argentina. (lsilva@ieee.org)

\* Grupo de Electrónica Aplicada, Dpto de Electricidad y Electrónica, Facultad de Ingeniería, Universidad Nacional de Río Cuarto, Argentina.

Received: May 24, 2013; Accepted: October 22, 2013

It is composed of connected elements that highlight energy properties of the system. It allows determining systematically an inversion based control scheme. In [11] this approach is used to model and control HEVs.

After defining the vehicle model and its representation, different analyses can be conducted via simulation. Within the large variety of simulation tools devoted to EVs and HEVs, Advisor [12] and QSS-TB [13] are aimed to develop quasi steady-state models and have been used successfully to evaluate fuel consumption and its optimization [14].

In [15] it is used Matlab/Simulink to construct dynamic models which is a flexible simulation tool where the user can define and program each component of the vehicle.

More specific tools incorporate libraries oriented to model EVs and HEVs such as Dymola [16] and PSAT [17].

Finally there are specific softwares in which the modeling is carried out by interconnecting predefined blocks making the procedure faster but less flexible. In [18] it is used PSIM whereas in [19] it is used Carsim.

The goal of this paper is to develop a complete 3-D representation of a four wheels EV (see Fig.1) using a structural energy-based approach whereas its control is represented using a functional description. In this way, the advantages of each approach are better exploited. This idea is inspired by [20] where a first coupling between a structural and a functional approach is proposed.

In this work a power system is simulated using PSIM (with a structural component library) and the control is designed using the EMR (functional approach). Also in [21] it is studied the advantage of using BG for representing the system and block diagrams for representing the controller.

Here the BG model is only used to obtain the dynamic equations of the powertrain but then the entire system (vehicle and control) is simulated in Matlab / Simulink using block diagrams (i.e. the structural approach is lost).

To meet the goal, in our proposal, the 3-D mechanics and the electric traction system of the vehicle are modeled with MBG and its control is described in block diagrams. In order to simulate the complete system behavior, the vehicle model and its control are integrated in the same simulation environment.

Models of the 3-D mechanical behavior of vehicles using BG were already presented in [22]. In [23] the translational and rotational dynamics are grouped and modeled together by mean of the MBG reducing significantly these models but the electromechanical interaction was neither modeled nor analyzed. To include this interaction, BG-based models of EVs and HEVs were presented in [24]. They include a BG model of the electric motor but the mechanical behavior is reduced to longitudinal dynamics only. Thus the proposed model in this work complements those models presented in recent literature.

## Nomenclature

| Parameters and Variables from Mechanical Domain |                               |
|---|-------------------------------|
| $\mathbf{T}$                                    | Torque (vector)               |
| $\mathbf{F}$                                    | Force (vector)                |
| $\boldsymbol{\omega}$                           | Angular velocity (vector)     |
| $\mathbf{v}$                                    | Velocity (vector)             |
| $\mathbf{x}$                                    | Displacement (vector)         |
| $\delta$  | Steering angle                |
| $r_w / I_w$                                     | Tire radius/inertia           |
| $m_w$   | Unsprung mass (at each wheel) |
| $k_t$   | Tire vertical stiffness       |
| $k_s / B_s$                                     | Suspension stiffness/damping  |
| $m$   | Vehicle mass                  |
| $I_{xx} / I_{yy} / I_{zz}$                      | Roll/Yaw/Pitch inertia        |
| $\phi / \psi / \theta$                          | Roll/Yaw/Pitch angles         |
| $C_{drag}$                                      | Aerodynamic coefficient       |
| $\rho$  | Air density                   |
| Parameters and Variables from Electrical Domain |                               |
| $\lambda$                                       | Magnetic flux                 |
| $\theta_z$                                      | Rotor flux angle              |
| $v/i$   | Voltage/Current               |
| $\omega_{qd0}$                                  | Angular velocity (frame)      |
| $P$   | Pairs of poles                |
| $L_m$   | Magnetizing inductance        |
| $L_{ls} / L_{lr}$                               | Stator/Rotor leakage          |
| $R_s / R_r$                                     | Stator/Rotor resistance       |
| $T_s$   | Sample time (controller)      |

## 2. Mechanical Characteristics and Modeling

In this Section, the model of the vehicle is created using Dymola which is an integrated environment for developing models in the open Modelica language [25]. Dymola allows generating structural representations which consist of connected components. These components have “connectors” that describe the interaction possibilities, e.g. an electrical pin, a mechanical flange, or an input/output signal. By connecting components a physical system model can be constructed. Dymola includes libraries to generate BG and MBG models. In 3-D mechanical applications, elements are represented compactly using MBG. Three single bonds are grouped into a Multi-Bond representing the rotational dynamics and another Multi-Bond is used for describing the translational dynamics.

Chassis and suspensions are modeled using the “Modelica library for MBGs and its application in 3-D mechanics” [26]. These components are internally represented with elements of the MBG library and are provided with external frames where the rotational and translational Multi-bonds are connected. The mechanical connection between two 3-D components is made via their

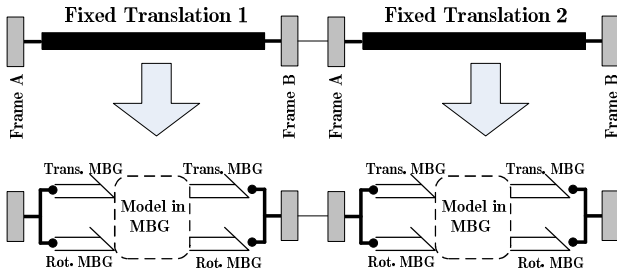


**Fig. 2.** Connection of two different 3-D mechanical elements.

frames that act as interfaces for exchanging power. As example, the upper part of Fig. 2 depicts the graphical representation of the connection of two 3-D components called “fixed translations” while the lower part shows that their internal models uses the MBG approach. The connection implies that both components have the same angular / linear velocities and positions at the connecting point.

## 2.1. Chassis

The model of the chassis contains a sprung mass that behaves like a lumped mass for the translational dynamics whereas for the rotational dynamics it contains the inertia tensor thus acting like a rigid body. The laws for the 3-D body motion are given by the Euler's equations

$$\mathbf{F} = m \cdot \mathbf{a} \quad (1)$$

$$\mathbf{T} = \left( \frac{d\mathbf{L}}{dt} \right)_{local} + \boldsymbol{\omega} \times \mathbf{L} \quad (2)$$

$$\mathbf{L} = \mathbf{I}_{CH} \cdot \boldsymbol{\omega} \quad (3)$$

where  $\mathbf{F} = [F_x \ F_y \ F_z]^T$  and  $\mathbf{T} = [T_x \ T_y \ T_z]^T$  are the forces (in the global frame) and torques (in the local frame) applied over the rigid body, respectively. Also,  $m$  and  $\mathbf{a}$  represent the mass and acceleration of the chassis. Moreover,  $\mathbf{L}$ ,  $\boldsymbol{\omega}$  and  $\mathbf{I}_{CH}$  represent the angular momentum, angular velocity and moment of inertia tensor of the chassis, respectively. Fig. 3 shows the 3-D body representation together with its internal representation in MBG.

To complete the chassis model “Fixed translations” are needed. They are ideal undeformable rods considered massless. Forces and velocities are given in the global

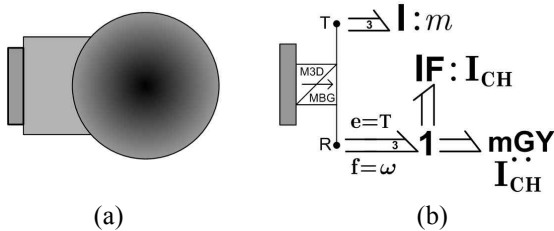


**Fig. 3.** (a) Free body in 3-D mechanics, (b) Internal composition in MBG.

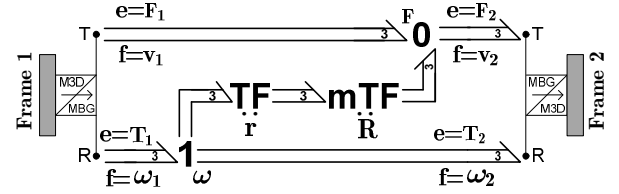


**Fig. 4.** Internal representation of fixed translations in MBG.

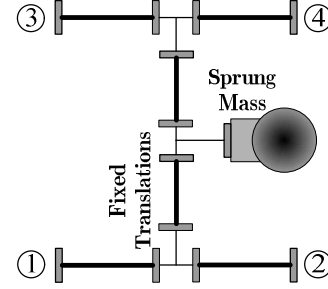


**Fig. 5.** Complete chassis modeled with 3-D mechanics components.

frame whereas torques and angular velocities in the local frame. The set of equations is given by

$$\mathbf{v}_2 = \mathbf{v}_1 + \mathbf{R} \cdot (\boldsymbol{\omega} \times \mathbf{r}) ; \mathbf{F}_2 = \mathbf{F}_1 \quad (4)$$

$$\mathbf{T}_1 = \mathbf{T}_2 + \mathbf{r} \times \mathbf{R}^T \cdot \mathbf{F} ; \boldsymbol{\omega}_1 = \boldsymbol{\omega}_2 \quad (5)$$

where  $\mathbf{R}$  and  $\mathbf{r}$  are the orthonormal orientation matrix and the vector that links both frames, respectively. The representation in 3-D mechanics is depicted in Fig. 2 and its internal MBG representation is presented in Fig. 4. Eq. (4) is graphically expressed in the “0” of the upper part whereas Eq. (5) is in the “1” of the lower part.

Fig. 5 shows the complete chassis model. Here a set of fixed translations is used to compose the undeformable structure of the chassis that projects the efforts and flows from the sprung mass -located in the center of gravity toward the points where the suspensions are mechanically connected in the frames noted with ①, ②, ③ and ④.

## 2.2. Suspension

The suspension system is composed by four suspensions that couple each wheel to the chassis. Fig. 6(a) shows that each suspension contains an ideal spring and a damper (from the 3-D mechanics library) which are connected according to the real mechanical configuration.

Spring force ( $\mathbf{F}_k$ ), damper force ( $\mathbf{F}_B$ ) and total suspension force ( $\mathbf{F}_{susp}$ ) are given by

$$\mathbf{F}_k = -k_s \Delta \mathbf{x} = -k_s \Delta \mathbf{x} \quad (6)$$

$$\mathbf{F}_B = -B_s (\mathbf{v}_2 - \mathbf{v}_1) = -B_s (\mathbf{v}_2 - \mathbf{v}_1) \quad (7)$$

$$\mathbf{F}_{susp} = \mathbf{F}_B + \mathbf{F}_k \quad (8)$$

where velocities on frames 1 and 2 are  $\mathbf{v}_1$  and  $\mathbf{v}_2$  and  $\Delta \mathbf{x}$  is

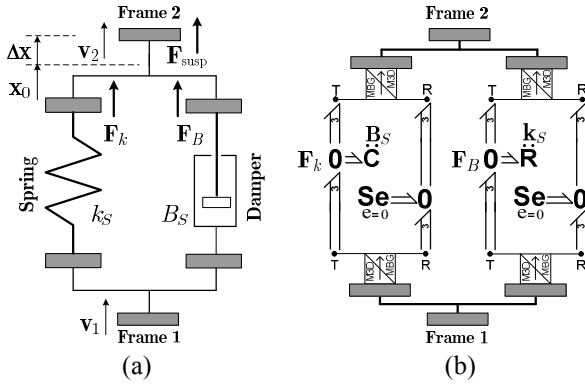


Fig. 6. (a) 3-D mechanical model, (b) Internal composition in MBG.

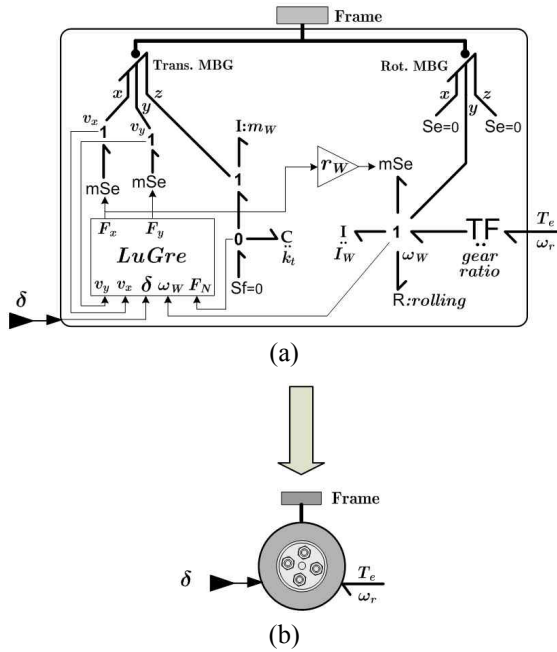


Fig. 7. (a) BG-MBG internal model of the wheel, (b) 3-D mechanical representation.

the displacement respect to the rest position ( $\mathbf{x}_0$ ).

The suspension stiffness and damper coefficient matrices are  $\mathbf{k}_S = -k_S \mathbf{I}_{3 \times 3}$  and  $\mathbf{B}_S = B_S \mathbf{I}_{3 \times 3}$ , respectively. Fig. 6(b) depicts the internal model in MBG.

### 2.3. Wheel and tires

Fig. 7(a) contains the Dymola internal model of the wheel that includes the calculation of the normal force at the contact patch ( $F_N$ ) based on a BG model of the vertical dynamics.

The longitudinal / lateral forces ( $F_x / F_y$ ) depend on the tire characteristics and certainly influence the dynamic behavior of the vehicle. These forces are determined using a 2-D LuGre friction model [27] that is widely used to estimate and control the traction contact force [28]. It allows representing different road conditions and the

transient behavior of the traction forces with a concise model that considers the coupling between  $x$  and  $y$  directions. Rotational dynamics is represented in a BG model that receives the torque ( $T_e$ ) generated by the Induction Machine (IM) and calculates its angular speed ( $\omega_r$ ). The torque balance also includes: rolling resistance, inertia momentum of the wheel ( $I_W$ ) and the opposition torque due to the longitudinal force on the patch contact at distance  $r_W$ . Then, translational dynamics along three axes are grouped into a multi-bond, as well as rotational dynamics.

These multi-bonds are used to incorporate the 3-D mechanical frame. Fig. 7(b) shows the Dymola 3-D mechanics model. It contains a mechanical frame to connect with the suspension, a single bond to interact with the IM and receives the steering signal ( $\delta$ ).

### 3. Electric Traction System

Two identical IM drive the rear wheels which are controlled independently. This feature allows the implementation of yaw stability control [29, 30] using a simple strategy to estimate the sideslip angle [31].

The set of equations concerning voltage and flux linkage in  $qd$  coordinates together with the equivalent circuit are given in [32]. The  $qd$  coordinates representation means that all variables are referred to an arbitrary reference frame rotating with angular velocity  $\omega_{qd0} = d\rho/dt$ . Angle  $\rho$  is the d-axis position. Electromagnetic torque ( $T_e$ ) as function of electrical variables, obtained with the power invariant transformation, is given by

$$T_e = P L_m (i_{qs}' i_{dr}' - i_{ds}' i_{qr}') \quad (9)$$

to represent the power interaction between electrical and mechanical domains modulated gyrators (**MGY**) were used, see Fig. 8. From Fig. 8(a) the following equation can be derived

$$e'_{qr} = P \lambda'_{dr} \omega_r ; \quad e'_{dr} = P \lambda'_{qr} \omega_r \quad (10)$$

Taking into account that the **MGY**'s do not add or dissipate power and using the power conservation at the "1" the following equation can be obtained

$$T_e \omega_r = i'_{dr} e'_{dr} - i'_{qr} e'_{qr} \quad (11)$$

Replacing (10) into (11) an alternative expression for  $T_e$  is

$$T_e = P (\lambda'_{qr} i'_{dr} - \lambda'_{dr} i'_{qr}) \quad (12)$$

It can be proved that Eq. (12) is equivalent to (9), thus

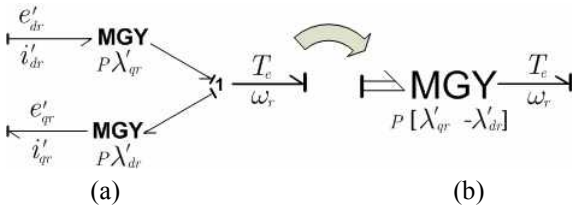


**Fig. 8.** BG diagram used to couple electrical and mechanical domains.

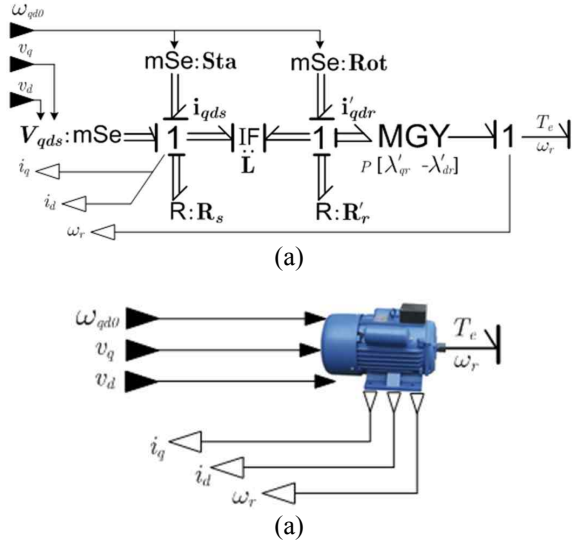


**Fig. 9.** (a) MBG representation; (b) Wrapped model in Dymola.

the **MGY** presented in Fig. 8(b) can be used to couple the electrical and mechanical domains.

To keep consistency with the mechanical model, the IM equivalent circuit was represented in a MBG of cardinality two. The resulting model is presented in the compact diagram shown in Fig. 9(a) together with its Dymola representation in Fig. 9(b). Variables and parameters are

$$\begin{aligned} \mathbf{R}_s &= R_s \mathbf{I}_{2 \times 2} \\ \mathbf{R}_r &= R_r \mathbf{I}_{2 \times 2} \\ \mathbf{L} &= \begin{bmatrix} (L_{ls} + L_m) & L_m \\ L_m & (L_{lr} + L_m) \end{bmatrix} \\ \mathbf{Sta} &= [\omega_{qd0} \lambda_{qs} - \omega_{qd0} \lambda_{ds}]^T \\ \mathbf{Rot} &= [\omega_{qd0} \lambda'_{qr} - \omega_{qd0} \lambda'_{dr}]^T \end{aligned}$$

For the case of study, electric variables are expressed using a  $qd$  stationary frame ( $\omega_{qd0} = 0$ ). Variables in this frame are noted as  $\alpha\beta$  variables.

#### 4. Integrated Model

This Section is devoted to generate the integrated model which includes in the same simulation environment the

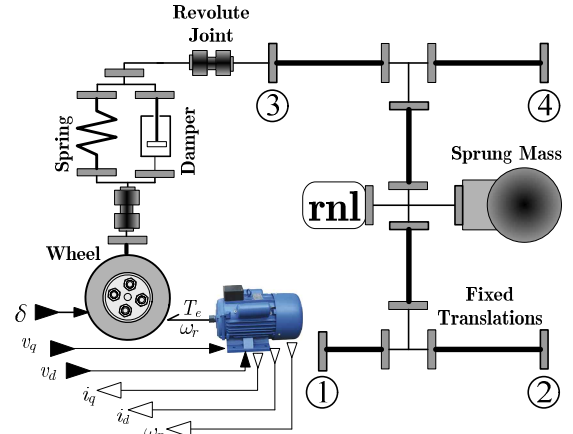


**Fig. 10.** Complete connection of Wheel and Suspension in Dymola.

complete model of the vehicle (with a structural representation in Section IV-A) and the controllers (with a functional representation in Section IV-B).

#### 4.1 Complete model of the vehicle

In order to obtain the structural representation of the entire vehicle, the mechanical and electrical sub-systems were interconnected. Each suspension and the chassis are connected through a revolute joint, which permits relative rotation along one axis. It also allows the chassis pitch movement while each suspension remains in vertical position. Similarly the lower end of the suspension system connects to the wheel's frame through a revolute joint. This connection allows the spinning of the wheel. Fig. 10 shows the complete connection of the left rear wheel and suspension. Connections of the other three wheels are analogous (front wheels do not have traction motor). It was also incorporated a non-linear resistance “**rnl**” that models the dragging force along the longitudinal direction.

#### 4.2 Control Scheme

The most adequate approach used to describe a control scheme is a functional representation. This Section presents the scheme implemented in the prototype which gives a clear overall description. Additionally, each block is internally programmed giving hierarchical levels of descriptions.

In order to emulate a mechanical differential, an equal torque strategy is proposed. This strategy is implemented by the Electronic Differential System (EDS), see Fig. 11, which determines the reference torque to be applied by each IM. Based on this reference torque a Field Oriented Control (FOC) was implemented on each motor, see Fig. 12. A well detailed description of the EDS/FOC strategy is given in [33]. It is proposed a simple strategy. More complex controllers regarding an EDS are presented in [34].



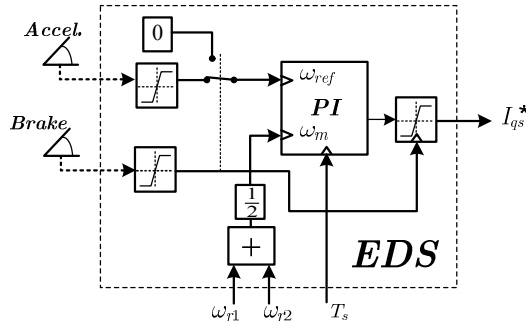


Fig. 11. Block Diagram representation of the EDS.

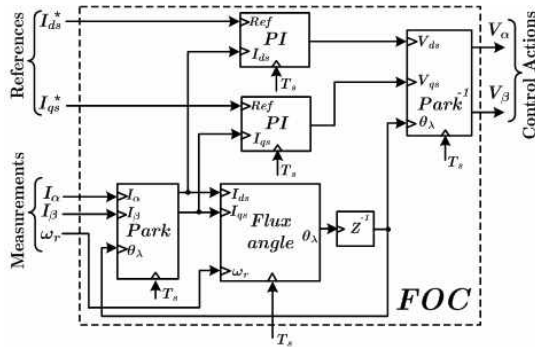


Fig. 12. Block Diagram representation of the FOC.

#### 4.3 Integration of structural / functional representations

The final part of the proposal consists on coupling the vehicle model with its control in the same simulation environment in order to study the complete vehicle performance.

The physical system model, built in Dymola, is compiled by Modelica and exported to the Matlab/Simulink environment. To this end, the model (see Fig. 10) is provided with the inputs / outputs necessary to interact in Simulink. Inputs are the steering angle ( $\delta$ ) and the reference  $\alpha\beta$  voltages applied to the IMs. Currents and rotor angular speed are the outputs used to implement both FOCs. The control algorithm is obtained in Simulink to close the control loop.

The integrated model which combines both approaches is displayed in Fig. 13. It shows explicitly that the inputs are the driver commands and the outputs can be any physical variable of interest.

The resulting model allows evaluating different controllers in a simulation environment, but using a complete vehicle model. Thus, any modification in the controller configuration or in its adjustment can be easily tested under simulation. Once the control algorithm has been tuned, it can be transferred to the digital controller using toolboxes that allow directly translating the control algorithm to a particular digital processor [35]. These toolboxes generate optimized C code for DSP / FPGA from plain Simulink diagrams.

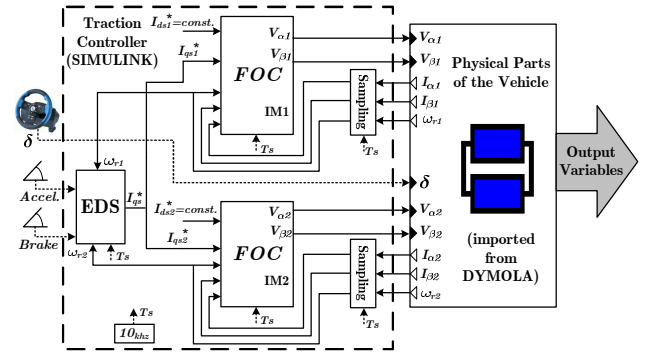


Fig. 13. Block Diagram representation of the FOC.

Additionally, BG allows us to modify quickly the physical model of the vehicle before producing any change in the actual prototype. Thus, the impact of such changes (e.g. tires, suspensions) over the controller or the overall vehicle performance can be verified and evaluated immediately, at practically no cost. Once the modifications have been tested and the results are satisfactory, they can be implemented in the actual vehicle prototype.

#### 5. Simulations Results and Experimental Validations

The first part (Section V-A) provides simulation and experimental results that validate the proposed model.

Table 1. Vehicle model parameters.

| Mechanical Domain                          |                         |
|--|-------------------------|
| Aerodynamic Coefficient ( $C_{drag}$ )     | 0.5                     |
| Frontal area ( $A_f$ )                     | 1.4 m <sup>2</sup>      |
| Air density ( $\rho$ )                     | 1.225 kg/m <sup>3</sup> |
| Vehicle mass with two passengers ( $m$ )   | 960 Kg                  |
| Tires, type and dimensions                 | 14570R13S               |
| Tread distance ( $l$ )                     | 1.10 m                  |
| Distance from CG to front axes ( $a$ )     | 1.02 m                  |
| Distance from CG to rear axes ( $b$ )      | 0.68 m                  |
| Pneumatic tire radius (unloaded) ( $r_w$ ) | 0.268 m                 |
| Unsprung mass (at each wheel) ( $m_w$ )    | 38.42 kg                |
| Tire vertical stiffness ( $k_t$ )          | 150000 Nm               |
| Tire inertia ( $I_w$ )                     | 1.95 kgm <sup>2</sup>   |
| Damper coefficient ( $B_s$ )               | 483 Ns/m                |
| Suspension stiffness ( $k_s$ )             | 23600 Nm                |
| Yaw Inertia ( $I_{yy}$ )                   | 352 kgm <sup>2</sup>    |
| Pitch Inertia ( $I_{zz}$ )                 | 356 kgm <sup>2</sup>    |
| Roll Inertia ( $I_{xx}$ )                  | 152 kgm <sup>2</sup>    |
| Electrical Domain                          |                         |
| Rated Power                                | 2x(3kW-4HP)             |
| Rated line voltage                         | 28 V <sub>rms</sub>     |
| Rated current                              | 81.56 Arms              |
| Pairs of poles ( $P$ )                     | 2                       |
| Rated rotor speed                          | 1455 RPM                |
| $R_s$                                      | 10.476 mΩ               |
| $R'_r$                                     | 22.231 mΩ               |
| $L_m$                                      | 1.21 mH                 |
| $L_{ls} / L'_{lr}$                         | 89.03 μH                |

Then in Section V-B only simulation results are given in order to highlight potential applications of the proposed methodology. These results are obtained using the scheme presented in Fig. 13. Parameters of the mechanical and electrical submodels are shown in Table 1.

## 5.1. Model validation

### 5.1.1 Acceleration-Brake

This experiment is aimed to evaluate the electro-mechanical power interaction. The vehicle was conducted from rest to the maximum speed and then back to rest. This sequence was performed twice. Fig. 14 shows simulation and experimental results of IM1. Maximum  $\omega_1 \approx 1050$  rpm corresponds to  $Vx \approx 30$  km/h. In Fig. 15 the consumed electric power of IM1 is depicted. Its negative value during braking, evidences the regenerative braking capability. The correlation between experimental and simulation results ensures a correct prediction of the energy consumed for any driving cycle.

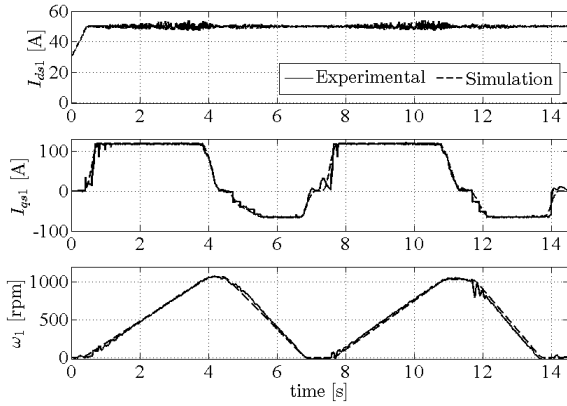


Fig. 14. Simulation/experimental results for Acceleration-Brake.

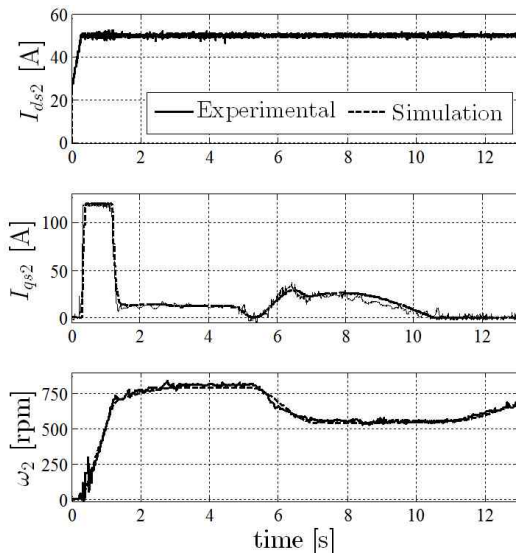
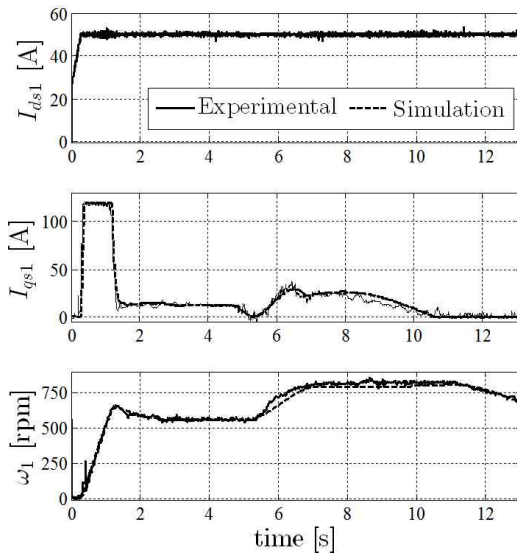


Fig. 17. Simulation and experimental results for the turning maneuver experiment: (a) Right and (b) left wheel motor.

Along the complete maneuver the total energy demanded to drive the vehicle is  $\approx 97.8$  kJ whereas the recovered energy is  $\approx 29.9$  kJ. From these results it is possible to quantify the improvement of the energetic efficiency which is approximately 30.56%.

### 5.1.2 Turning Maneuver

Figs. 16 and 17 show simulation and experimental results of the steering angle and IMs variables obtained in this experiment.

The vehicle began stopped and then accelerated and remained at constant speed. Fig. 16 shows that the vehicle first turned right, then it turned left and came back to a straight direction. Fig. 17 shows that while the vehicle was

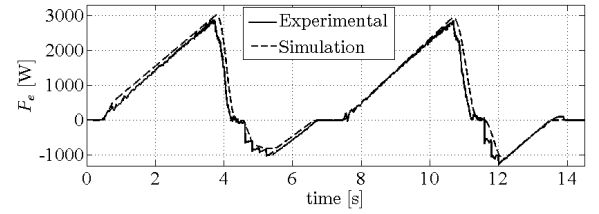


Fig. 15. Electric power during the Acceleration-Brake.

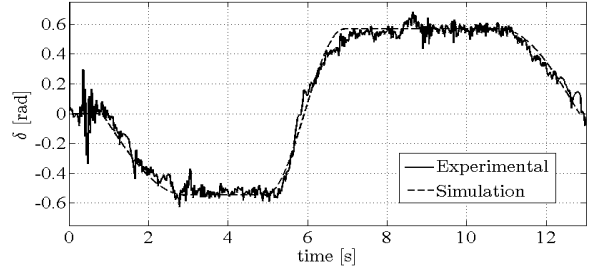
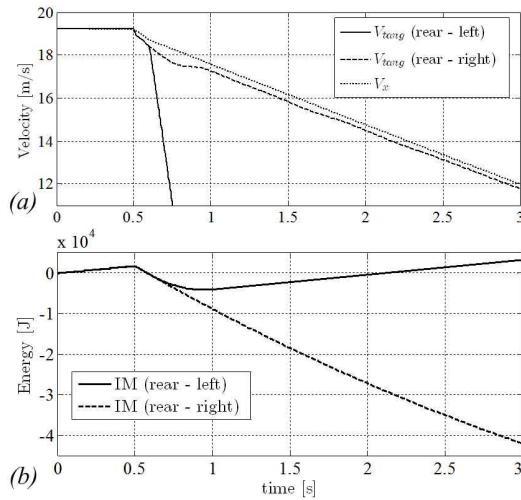


Fig. 16. Steering angle evolution during the turning maneuver.



**Fig. 18.** (a) Velocities during blockage, (b) IMs energy flow.

turning right, the inner curve wheel speed (IM1) was smaller than that of the outer one (IM2) and then it changed as the vehicle direction changed. During the whole experiment, wheel torques (proportional to  $I_{qs}$ ) were the same for both motors as expected due to the implemented EDS algorithm.

The largest difference in Fig. 17 can be seen for  $I_{qs}$  (mean squared error of 3.96%). Simulation and experimental results during the turning maneuver presented EDS algorithm. The largest difference in Fig. 17 can be a mean squared error smaller than 4% for all variables. The inclusion of lateral dynamics allows reproducing turning maneuvers with high fidelity. This property is necessary to evaluate the vehicle maneuverability and stability under dangerous conditions. Furthermore, it helps to design vehicle yaw controllers and test their performance.

## 5.2. Potential applications

Results presented in this section emphasize the capability of the model to simulate dangerous situations and/or variables difficult or impossible to measure. Fig. 18 (a) shows an experiment where both left wheels were blocked during braking. The vehicle was driven at a constant speed of 70 km/h and after 0.5 seconds the brake was applied (mechanical brake on frontal wheels). At  $t = 0.6$  s, road condition for left wheels was changed to extremely slippery, producing their blockage. Right wheels kept braking along producing a net torque. The vehicle continued to slow down as shown in Fig. 18(a) but the tangential velocities of the blocked and non-blocked wheels were absolutely different.

Because of the wheel blockage, the regenerative braking capability of the IM was lost in the left rear wheel (continuous line in Fig. 18(b)) whereas the IM located on right rear wheel (dashed line in Fig. 18(b)) kept recovering energy.

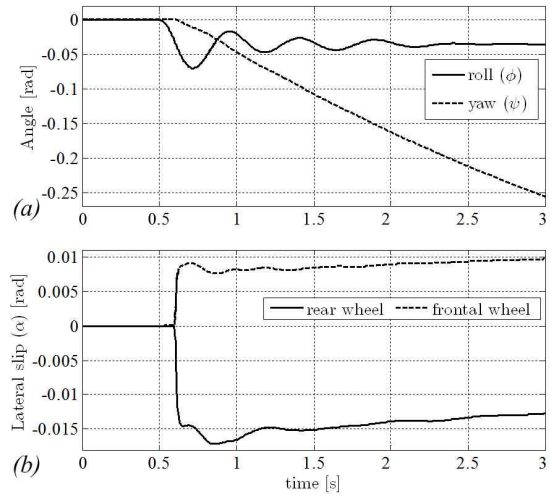


**Fig. 19.** (a) Roll and yaw evolution during blockage, (b) Lateral slip of rear and frontal wheels during blockage.

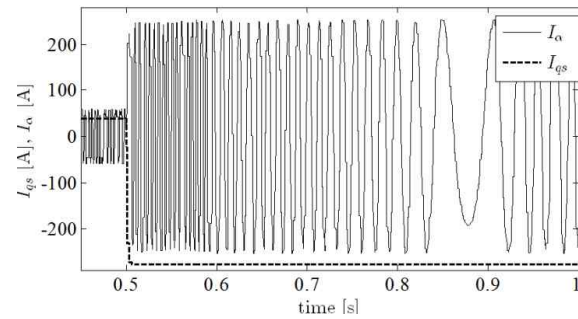


**Fig. 20.** Currents behavior during blockage experiment.

An important yaw angle appeared (Fig. 19(a)) due to asymmetry on the longitudinal forces. This yaw rate ( $\dot{\psi}$ ) produced load transference toward the left side and a negative roll angle occurred. Lateral slip is seen in Fig. 9(b).

Variables of the FOC presented in Section IV-B are depicted in Fig. 20. They are the measured  $I_\alpha$  and the Park transformed  $I_{qs}$  in the IM connected to the blocked wheel.

Simulation results illustrate the wide range of applications possible to tackle. It is possible to assess the response during risky situations, power flow between electric and mechanical domains and variables regarding the control.

Moreover, the behavior of the tire-road interaction can be studied. These variables are needed to estimate and control the traction contact forces. In [28] the longitudinal dynamics of the proposed model was successfully used to this end.

## 6. Conclusion

A novel simulation methodology based on a combination of structural (for the physical system) and



functional (for the controller) approaches oriented to developing electric vehicle (EV) concepts was proposed. A remarkable contribution of the proposal is that applying this combination it is possible to exploit the advantages of each approach.

The structural approach is based on Multi-Bond Graph (MBG) that allows representing each EV sub-system in a compact/modular way. This approach allows representing the power interactions between sub-systems independently of their physical nature. Moreover, the functional approach is accomplished using Block Diagrams (BD) that gives a clear overall description of the input/output relationships in the controller.

The proposed procedure consists on integrating both representations (represented in MBG and BD) into a single simulation environment. The resulting model allows evaluating and verifying rapidly any modification on the vehicle or in the controller, reducing time and development costs. The versatility of the proposal permits to implement other EV configurations and helps to understand the dynamics of electrically driven vehicles.

Experimental results were obtained using a real vehicle prototype. The high correlation between simulation and experimental results demonstrates the practical feasibility of the proposal.

## References

- [1] D. Gao, C. Mi, and A. Emadi, "Modeling and simulation of electric and hybrid vehicles," *Proc. of the IEEE*, vol. 95, no. 4, pp. 729-745, april 2007.
- [2] A. T. Kamil Çagatay Bayindir, Mehmet Ali Gözükcükük, "A comprehensive overview of HEV: Powertrain configurations, powertrain control techniques and electronic control units," *Energy Conversion and Management*, vol. 52, no. 2, pp. 1305-1313, 2011.
- [3] L. Wang, Y. Zhang, C. Yin, H. Zhang, and C. Wang, "Hardware in the loop simulation for the design and verification of the control system of a series-parallel hybrid electric city-bus," *Simulation Modelling Practice and Theory*, vol. 25, pp. 148-162, 2012.
- [4] C. Chan, A. Bouscayrol, and K. Chen, "Electric, hybrid, and fuel-cell vehicles: Architectures and modeling," *Vehicular Technology, IEEE Transactions on*, vol. 59, no. 2, pp. 589-598, feb. 2010.
- [5] P. Gawthrop and G. Bevan, "Bond-graph modeling," *Control Systems Magazine, IEEE*, vol. 27, no. 2, pp. 24-45, april 2007.
- [6] D. C. Karnopp, D. L. Margolis, and R. C. Rosenberg, *System Dynamics: Modeling And Simulation of Mechatronic Systems*. New York, USA: Wiley Intersciences, 2006.
- [7] J. Jang and C. Han, "Proposition of a modeling method for constrained mechanical systems based on the vector bond graph," *Journal of the Franklin Institute*, vol. 335, no. 3, pp. 451-469, 1998.
- [8] R. Schonfeld and G.-H. Geitner, "Power flow and information flow in motion control system," in *Proc. EPE-PEMC*, sept. 2004.
- [9] G.-H. Geitner, "Power flow diagrams using a bond graph library under simulink," in *IEEE Industrial Electronics, IECON 2006-32<sup>nd</sup> Annual Conference on*, nov. 2006, pp. 5282-5288.
- [10] A. Bouscayrol, B. Davat, B. de Fornel, B. Francois, J. P. Hautier, F. Meibody-Tabar, and M. Pietrzak-David, "Multimachine multiconverter system: application for electromechanical drives," *Eur. Phys. J., Appl. Phys.*, vol. 10, no. 2, pp. 131-147, May 2000.
- [11] L. Boulon, D. Hissel, A. Bouscayrol, O. Pape, and M. Pera, "Simulation model of a military HEV with a highly redundant architecture," *Vehicular Tech, IEEE Trans. on*, vol. 59, no. 6, pp. 2654-2663, july 2010.
- [12] K. Wipke, M. Cuddy, and S. Burch, "ADVISOR 2.1: a user-friendly advanced powertrain simulation using a combined backward/forward approach," *Vehicular Technology, IEEE Transactions on*, vol. 48, no. 6, pp. 1751-1761, Nov. 1999.
- [13] L. Guzzella and A. Amstutz, "CAE tools for quasi-static modeling and optimization of hybrid powertrains," *Vehicular Technology, IEEE Transactions on*, vol. 48, no. 6, pp. 1762-1769, Nov. 1999.
- [14] D. Somayajula, A. Meintz, and M. Ferdowsi, "Designing efficient hybrid electric vehicles," *Vehicular Technology Magazine, IEEE*, vol. 4, no. 2, pp. 65-72, june 2009.
- [15] M. Sekour, K. Hartani, A. Draou, and A. Allali, "Sensorless fuzzy direct torque control for high performance electric vehicle with four in-wheel motors," *Journal of Electrical Engineering and Technology*, vol. 8, no. 3, pp. 530-543, 2013.
- [16] B. Zupancic and A. Sodja, "Computer-aided physical multi-domain modelling: Some experiences from education and industrial applications," *Simulation Modelling Practice and Theory*, 2012, in Press.
- [17] H. Borhan, A. Vahidi, A. Phillips, M. Kuang, I. Kolmanovsky, and S. Di Cairano, "MPC-based energy management of a powersplit hybrid electric vehicle," *Control Systems Technology, IEEE Transactions on*, vol. 20, no. 3, pp. 593-603, may 2012.
- [18] S. Onoda and A. Emadi, "PSIM-based modeling of automotive power systems: conventional, EVs, and HEVs," *Vehicular Technology, IEEE Transactions on*, vol. 53, no. 2, pp. 390-400, march 2004.
- [19] R. Wang and J. Wang, "Fault-tolerant control with active fault diagnosis for 4W independently driven electric ground vehicles," *VT, IEEE Trans on*, vol. 60, no. 9, pp. 4276-4287, nov. 2011.
- [20] P. Delarue, A. Bouscayrol, and P. Barrade, "Energetic macroscopic representation and PSIM R\_ simulation: Application to a DC/DC converter input filter stability," in *Vehicle Power and Propulsion Con-*

- ference (VPPC), 2010 IEEE, sept. 2010, pp. 1-6.
- [21] J. P. Mihael Cipek, Danijel Pavkovic, "A control-oriented simulation model of a power-split hybrid electric vehicle," *Applied Energy*, vol. 101, pp. 121-133, 2013.
- [22] T. Bera, K. Bhattacharya and A. Samantaray, "Evaluation of antilock braking system with an integrated model of full vehicle system dynamics," *Simulation Modelling Practice and Theory*, vol. 19, no. 10, pp. 2131-2150, 2011.
- [23] L. Silva, G. Magallan, C. De Angelo, and G. Garcia, "Vehicle dynamics using multi-bond graphs: Four wheel electric vehicle modeling," in *Industrial Electronics, 2008. IECON 2008. 34th Annual Conference of IEEE*, nov. 2008, pp. 2846-2851.
- [24] M. Djeziri, R. Merzouki, and B. Bouamama, "Robust monitoring of an EV with structured and unstructured uncertainties," *Vehicular Tech, IEEE Trans. on*, vol. 58, no. 9, pp. 4710-4719, nov. 2009.
- [25] "Modelica Language Specification, version 3.3," may 2012.[Online].Available:  
<https://www.modelica.org/documents>
- [26] D. Zimmer and F. Cellier, "The modelica multi-bond graph library," in *Proc. 5th Int. Modelica Conference*, vol. 2, 2006, pp. 559-568.
- [27] E. Velenis, P. Tsiotras, C. Canudas-de Wit, and M. Sorine, "Dynamic tyre friction models for combined longitudinal and lateral vehicle motion," *Vehicle System Dynamics*, vol. 43, no. 1, pp. 3-29, 2005.
- [28] G. Magallán, C. De Angelo, and G. Garcia, "Maximization of the traction forces in a 2WD electric vehicle," *Vehicular Technology, IEEE Transactions on*, vol. 60, no. 2, pp. 369-380, Feb. 2011.
- [29] J.Kang, J. Yoo, and K. Yi, "Driving control algorithm for maneuverability, lateral stability, and rollover prevention of 4WD EV with independently driven front and rear wheels," *Vehicular Technology, IEEE Transactions on*, vol. 60, no. 7, pp. 2987-3001, sept. 2011.
- [30] W. Cho, J. Choi, C. Kim, S. Choi, and K. Yi, "Unified chassis control for the improvement of agility, maneuverability, and lateral stability," *Vehicular Technology, IEEE Transactions on*, vol. 61, no. 3, pp. 1008-1020, march 2012.
- [31] K. Nam, S. Oh, H. Fujimoto, and Y. Hori, "Estimation of sideslip and roll angles of electric vehicles using lateral tire force sensors through rls and kalman filter approaches," *Industrial Electronics, IEEE Transactions on*, vol. 60, no. 3, pp. 988-1000, march 2013.
- [32] L. Silva, G. Magallán, P. de la Barrera, C. De Angelo, and G. Garcia, "Modeling of EV dynamics with multi-bond graphs," in *Vehicle Power and Propulsion Conf. (VPPC'10), IEEE*, sept. 2010, pp. 1-7.
- [33] G. A. Magallán, C. H. De Angelo, and G. O. García, "A Neighborhood Electric Vehicle Development with Individual Traction on Rear Wheels," *Int. Journal of Electric and Hybrid Vehicles (IJEHV)*, vol. 2, no. 2, pp. 115-136, Oct. 2009.
- [34] R. Sampaio, A. Hernandez, V. do Valle Magalha andes Fernandes, M. Becker, and A. Siqueira, "A new control architecture for robust controllers in rear electric traction passenger HEVs," *Vehicular Tech, IEEE Trans on*, vol. 61, no. 8, pp. 3441-3453, oct. 2012.
- [35] R. Duma, P. Dobra, M. Abrudean, and M. Dobra, "Rapid prototyping of control systems using embedded target for TI c2000 DSP," in *Control & Automation. MED '07 Conf. on*, June 2007, pp. 1-5.



**L. I Silva** He received his MSc in Space Sciences and Technologies from the Lulea Tekniska Universitet, Sweeden in 2007 and his PhD in Engineering Sciences from Universidad Nacional de Río Cuarto, Argentina in 2012. Since 2012 he is a postdoctoral student at Universidad Nacional de Río Cuarto.

His research topics are oriented to modeling and simulation applied to electric and hybrid electric vehicles.



**G. A Magallán** He received the Electronic Engineer degree from the Universidad Tecnológica Nacional, Paraná, Argentina, in 2002 and the M.Sc. and Dr. Eng. degree from the Universidad Nacional de Río Cuarto, Río Cuarto, Argentina, in 2009 and 2010, respectively. He is also with the Consejo

Nacional de Investigaciones Científicas y Técnicas, Buenos Aires, Argentina. His research interests include traction control of electric vehicles, dsp-based implementations, hybrid electric energy storage systems.



**P. M. De la Barrera** He received the B.Sc. and M.Sc. degrees in electrical engineering from Universidad Nacional de Río Cuarto, Río Cuarto, in 2003 and 2006, respectively, and the Ph.D. degree from Universidad Nacional del Sur, Bahía Blanca, Argentina, in 2009. Since 1998, he has been with the

Grupo de Electrónica Aplicada, Universidad Nacional de Río Cuarto. He is also currently with Consejo Nacional de Investigaciones Científicas y Técnicas, Buenos Aires, Argentina. His research interests include modelling, control and fault diagnosis of electric machines, ac motor drives, electric vehicles, and renewable energy generation.



**C. H. De Angelo** He received the Electrical Engineer degree from the Universidad Nacional de Río Cuarto, Río Cuarto, Argentina, in 1999 and the Dr. Eng. degree from the Universidad Nacional de La Plata, La Plata, Argentina, in 2004. In 1994, he joined the Grupo de Electrónica Aplicada,

Universidad Nacional de Río Cuarto. He is also with the Consejo Nacional de Investigaciones Científicas y Técnicas, Buenos Aires, Argentina. His research interests are fault diagnosis of electric machines, sensorless motor control, electric vehicles, and renewable-energy generation.



**G. O. García** He received the Electrical and Electronics Engineering degree from the Universidad Nacional de Córdoba, Córdoba, Argentina, in 1981 and the M.Sc. and Dr. degrees in electrical engineering from COPPE, Universidade Federal do Rio de Janeiro, Rio de Janeiro, Brazil, in 1990 and

1994, respectively. Since 1994, he has been with the Universidad Nacional de Río Cuarto, Río Cuarto, Argentina, where he is currently the Director of the Grupo de Electrónica Aplicada. He is also with the Consejo Nacional de Investigaciones Científicas y Técnicas, Buenos Aires, Argentina. His research interests include power electronics, electric vehicles, and renewable energy conversion.